Analysis of the bite force and mechanical design of the feeding mechanism of the durophagous horn shark *Heterodontus francisci*

Daniel R. Huber[1],*, Thomas G. Eason[2], Robert E. Hueter[3] and Philip J. Motta[1]

[1]*Department of Biology, University of South Florida, 4202 E. Fowler Avenue, SCA 110, Tampa, FL 33620, USA,*
[2]*Department of Mechanical Engineering, University of South Florida, 4202 E. Fowler Avenue, ENB 118, Tampa, FL 33620, USA* and [3]*Center for Shark Research, Mote Marine Laboratory, 1600 Ken Thompson Parkway, Sarasota, FL 34236, USA*

*Author for correspondence (e-mail: drhuber@mail.usf.edu)

Summary

Three-dimensional static equilibrium analysis of the forces generated by the jaw musculature of the horn shark *Heterodontus francisci* was used to theoretically estimate the maximum force distributions and loadings on its jaws and suspensorium during biting. Theoretical maximum bite force was then compared with bite forces measured (1) voluntarily *in situ*, (2) in restrained animals and (3) during electrical stimulation of the jaw adductor musculature of anesthetized sharks. Maximum theoretical bite force ranged from 128 N at the anteriormost cuspidate teeth to 338 N at the posteriormost molariform teeth. The hyomandibula, which connects the posterior margin of the jaws to the base of the chondrocranium, is loaded in tension during biting. Conversely, the ethmoidal articulation between the palatal region of the upper jaw and the chondrocranium is loaded in compression, even during upper jaw protrusion, because *H. francisci*'s upper jaw does not disarticulate from the chondrocranium during prey capture. Maximum *in situ* bite force averaged 95 N for free-swimming *H. francisci*, with a maximum of 133 N. Time to maximum force averaged 322 ms and was significantly longer than time away from maximum force (212 ms). Bite force measurements from restrained individuals (187 N) were significantly greater than those from free-swimming individuals (95 N) but were equivalent to those from both theoretical (128 N) and electrically stimulated measurements (132 N). The mean mass-specific bite of *H. francisci* was greater than that of many other vertebrates and second highest of the cartilaginous fishes that have been studied. Measuring bite force on restrained sharks appears to be the best indicator of maximum bite force. The large bite forces and robust molariform dentition of *H. francisci* correspond to its consumption of hard prey.

Key words: bite force, elasmobranch, feeding biomechanics, performance, durophagy, jaw suspension, *Heterodontus francisci*.

Introduction

The elasmobranch fishes (sharks, skates and rays) possess highly diverse feeding mechanisms composed of few kinetic elements, making them an ideal group in which to investigate feeding biomechanics and patterns of diversity in cranial morphology, feeding behavior and ecology. Elasmobranchs inhabit nearly all marine environments and have evolved ram, suction, biting and filter feeding mechanisms to exploit prey ranging from plankton to marine mammals (Motta, 2004). Among the diverse feeding mechanisms found in extant elasmobranch taxa are those adapted for durophagy, the consumption of hard prey. While 'hard' prey of some sort is found in the diets of elasmobranchs from approximately 13 families, it does not comprise a substantial portion of the diet in many of these groups. Genuine durophagy has convergently evolved in the bullhead (Heterodontidae), hammerhead (Sphyrnidae), zebra (Stegostomatidae) and hound sharks (Triakidae), as well as the eagle rays (Myliobatidae) (Compagno, 1984a,b, 2001; Summers et al., 2004).

The heterodontid sharks are the only family of elasmobranchs in which every species is ecologically and functionally specialized for durophagy (Compagno, 1984a, 1999; Taylor, 1972). The suite of morphological characters associated with durophagy in the heterodontid sharks includes robust jaws capable of resisting dorsoventral flexion under high loading, molariform teeth and hypertrophied jaw adductor muscles (Nobiling, 1977; Reif, 1976; Summers et al., 2004). To date, the concept of durophagy in the heterodontid sharks has mostly been examined qualitatively (but see Summers et al., 2004). Neither the bite forces they are capable of producing nor the subsequent loadings on the various articulations within their feeding mechanisms have been quantified in *any* manner. Bite force is particularly informative in regard to linking morphological, ecological and behavioral variables associated

with prey capture because biting capacity is dictated by cranial morphology and is known to affect resource partitioning (Verwaijen et al., 2002; Wiersma, 2001), dietary diversity (Clifton and Motta, 1998; Wainwright, 1988) and ontogenetic changes in feeding ecology (Hernandez and Motta, 1997).

Like most modern elasmobranchs, the heterodontid sharks possess a hyostylic jaw suspension in which the mandibular arch indirectly articulates with the chondrocranium *via* the hyomandibular cartilages, and the palatal region of the upper jaw is suspended from the ethmoid region of the chondrocranium *via* ligamentous connections (Fig. 1A). However, a number of variants on this arrangement exist, primarily in the superorder Squalea (Gregory, 1904; Shirai, 1996; Wilga, 2002). The hexanchiform sharks possess an orbitostylic jaw suspension in which the upper jaw articulates with the ethmoidal, orbital and postorbital regions of the chondrocranium, and the hyomandibula contributes little support to the jaws (Fig. 1B). Conversely, the only suspensorial element in the batoids is the hyomandibula (euhyostyly; Fig. 1C; Gregory, 1904; Maisey, 1980; Wilga, 2002). These highly divergent morphologies constitute independent mechanical systems, perhaps with comparably divergent cranial loading regimes occurring during feeding. Determining these loading regimes will help to establish the link, if any, between elasmobranch jaw suspension and the functional diversity of their feeding mechanisms.
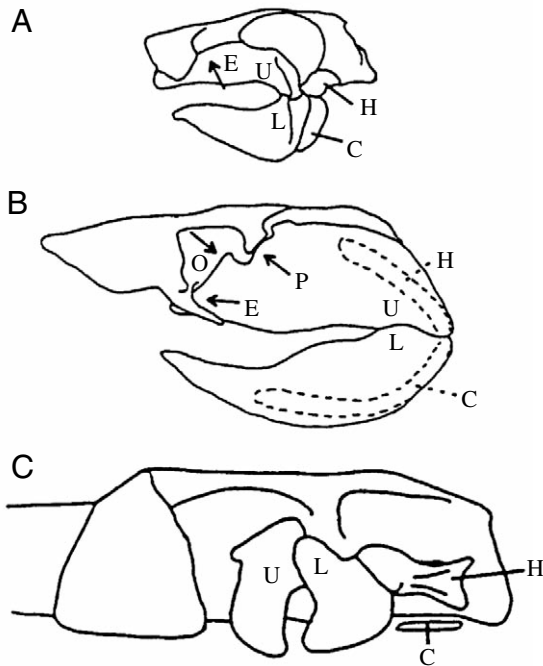

Fig. 1. Left lateral views of representative elasmobranch jaw suspensions. (A) *Heterodontus*, Heterodontiformes (hyostyly); (B) *Heptranchias*, Hexanchiformes (amphistyly); (C) *Rhinobatos*, Batoidea (euhyostyly). Articulation points are marked with arrows. C, ceratohyal; E, ethmoidal; H, hyomandibula; L, lower jaw; O, orbital; P, postorbital; U, upper jaw. Reproduced from Wilga (2002) with permission from Blackwell Publishing.

The purpose of this study was therefore to determine the biomechanical basis of durophagy in the heterodontid sharks, as represented by the horn shark *Heterodontus francisci* (Girard 1855), a primarily shallow-water, nocturnal forager of molluscs, echinoderms and benthic crustaceans (Segura-Zarzosa et al., 1997; Strong, 1989). *Heterodontus francisci* uses suction to capture prey, which is grasped by the anterior cuspidate teeth and then crushed by the posterior molariform teeth, effectively combining both suction and biting feeding mechanisms (Edmonds et al., 2001; Summers et al., 2004). Through *in situ* bite performance measurements and theoretical modeling of the forces generated by the cranial musculature of *H. francisci*, the specific goals of this study were to: (1) theoretically determine the forces generated by each of the cranial muscles active during the gape cycle; (2) determine the distribution of forces throughout the jaws and suspensorium and discuss the implications of these loadings for jaw suspension; (3) compare theoretical bite force from anatomical measures with those obtained during voluntary unrestrained feeding, restrained biting and electrical stimulation of the jaw adductors; (4) relate its bite performance to feeding ecology and (5) compare the bite force of *H. francisci* with those of other vertebrates.

Materials and methods
Experimental animals

Five horn sharks *Heterodontus francisci* Girard [63–74 cm total length (*TL*)] were housed at the University of South Florida in Tampa, FL, USA in accordance with the guidelines of the Institutional Animal Care and Use Committee (IACUC #1882). Individuals were maintained at 20°C in a 1500 liter semicircular tank on a diet of thread herring *Opisthonema oglinum* and squid *Loligo* spp. The planar face of the tank held a window for viewing. Five additional *H. francisci* (55–68 cm *TL*), obtained as fisheries bycatch off the coast of Los Angeles, CA, USA, were frozen until used for morphological analyses.

Morphological analysis

A theoretical model of the feeding mechanism of *H. francisci* was designed by investigating the forces produced by the nine cranial muscles involved in the abduction (coracomandibularis, coracohyoideus, coracoarcualis and coracobranchiales), adduction (adductor mandibulae complex consisting of the quadratomandibularis–preorbitalis complex, quadratomandibularis-γ and preorbitalis-α) and retraction (levator palatoquadrati and levator hyomandibularis) of the jaws and hyobranchial region (Fig. 2). The quadratomandibularis–preorbitalis complex consists of six individual heads of the adductor mandibulae complex (Nobiling, 1977). Difficulty in mechanically separating these heads led to their analysis as a group. Using the tip of the snout as the center of a three-dimensional coordinate system, the three-dimensional position of the origin and insertion of each muscle was determined by measuring the distance of these points from the respective *X*, *Y* and *Z* planes intersecting the
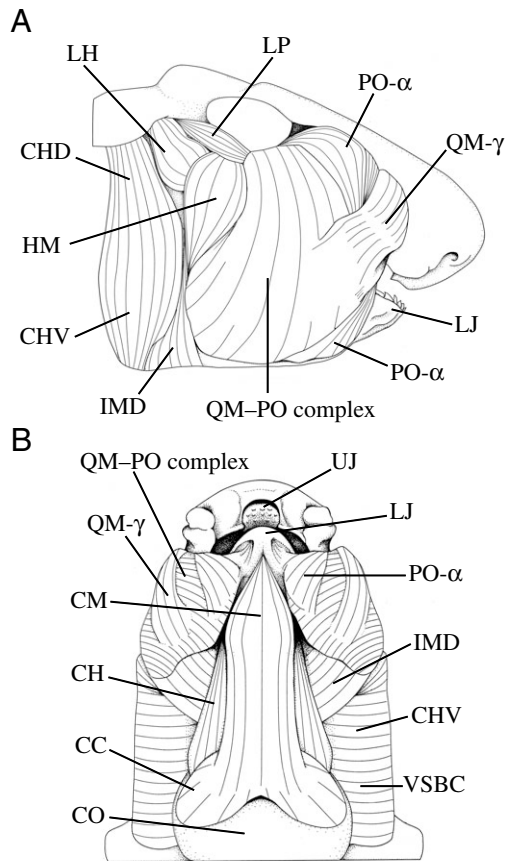
Fig. 2. Right lateral (A) and ventral (B) views of the cranial and branchial musculature of a 63 cm male *H. francisci*. CC, coracoarcualis; CH, coracohyoideus; CHD, dorsal hyoid constrictor; CHV, ventral hyoid constrictor; CM, coracomandibularis; CO, coracoid bar; HM, hyomandibulo-mandibularis; IMD, intermandibularis; LH, levator hyomandibularis; LJ, lower jaw; LP, levator palatoquadrati; QM–PO complex, quadratomandibularis–preorbitalis complex; QM-γ, quadratomandibularis-γ; PO-α, preorbitalis-α; UJ, upper jaw; VSBC, ventral superficial branchial constrictor. The IMD has been partially removed to reveal the ventral musculature. The coracobranchiales (not shown) are located deep to the CC.

tip of the snout (Fig. 3A). Each muscle was then excised (unilaterally where applicable), bisected through its center of mass perpendicular to the principal fiber direction, and digital images of the cross-sections were taken (JVC DVL9800 camera). Cross-sectional areas were measured from these images using Sigma Scan Pro 4.01 (SYSTAT Software Inc., Point Richmond, CA, USA). Center of mass was estimated by suspending the muscle from a pin and tracing a vertical line down the muscle. After repeating this from another point, the intersection of the two line-tracings indicated the center of mass of the muscle.

The three-dimensional coordinates of the center of rotation of the dual (lateral and medial; Nobiling, 1977) quadratomandibular jaw articulation (hereafter referred to as 'jaw joint'), the ethmoidal articulation and the lateral and medial articulations of the hyomandibula with the jaws and chondrocranium, respectively, were determined with respect to the right side of the head of each individual. Points corresponding to 0, 25, 50, 75 and 100% of the distance along the functional tooth row on the lower jaw from the posteriormost molariform tooth were also determined; 100% is the anteriormost cuspidate tooth. The in-lever for jaw abduction from the center of rotation of the jaw joint to the point of insertion of the coracomandibularis was determined from the three-dimensional coordinates. In-levers for jaw adduction from the center of rotation of the jaw joint to the points of insertion on the lower jaw of the quadratomandibularis–preorbitalis complex, quadratomandibularis-γ and preorbitalis-α were determined in the same manner. A weighted average of these in-levers was determined based on the forces produced by their respective muscles. The abductive and weighted adductive in-levers were divided by the out-lever distance from the center of rotation of the jaw joint to the tip of the anteriormost tooth of the lower jaw to determine mechanical advantage ratios for jaw opening and closing (Fig. 3B). Due to the quadratomandibularis–preorbitalis complex's broad surface attachment on the lateral face of both the upper and lower jaws, an exact insertion point for this muscle could not be identified.
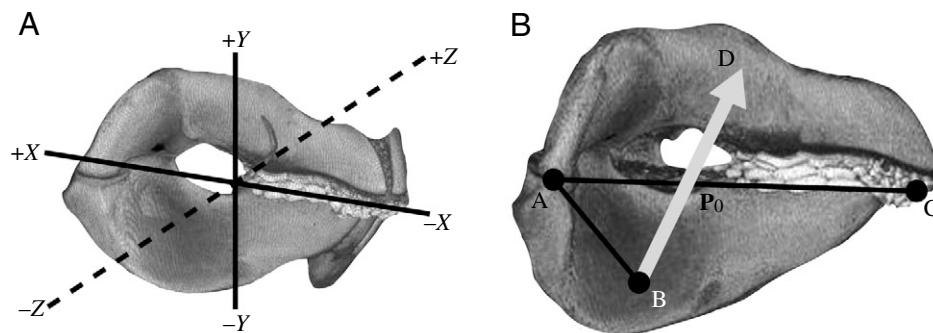

Fig. 3. (A) Coordinate system for three-dimensional vector analysis of the forces generated by the cranial musculature of *H. francisci*. Directionality is defined with respect to the head of *H. francisci* using the 'right-hand rule'. (B) Schematic diagram of the jaws of *H. francisci* indicating variables for mechanical lever-ratio analysis. A–B, resolved in-lever for jaw adduction; A–C, out-lever; B–D, resolved adductive muscle force vector; P_0, maximum tetanic tension. CT-scan image used with permission of A. Summers.

Its center of mass and principal muscle fiber direction relative to the lower jaw were used to approximate its mechanical line of action. The distance from the jaw joint to the intersection of this line of action with the lower jaw served as the in-lever for this muscle. Anatomical nomenclature is based on Daniel (1915), Motta and Wilga (1995, 1999) and Nobiling (1977).

Theoretical force generation

Anatomical cross-sectional area (A_{cs}) measurements of the nine parallel fibered muscles were multiplied by the specific tension of elasmobranch white muscle (T_{sp}; 289 kN m^{-2}; Lou et al., 2002) to determine their theoretical maximum tetanic forces (P_0):

$$P_0 = A_{cs} \times T_{sp} . \quad (1)$$

Anatomical cross-sectional area was used in this analysis because theoretical estimates of maximum bite force based on the anatomical cross-sectional area of the parallel fibered jaw adducting musculature of the spiny dogfish *Squalus acanthias* best approximated bite forces measured during tetanic stimulation of the jaw adducting musculature (Huber and Motta, 2004). Force vectors for each muscle were constructed from their maximum tetanic forces and the three-dimensional coordinates of their origins and insertions. The force vectors of muscles excised unilaterally were reflected about the *Y*-plane to represent the forces generated by the musculature on the other side of the head.
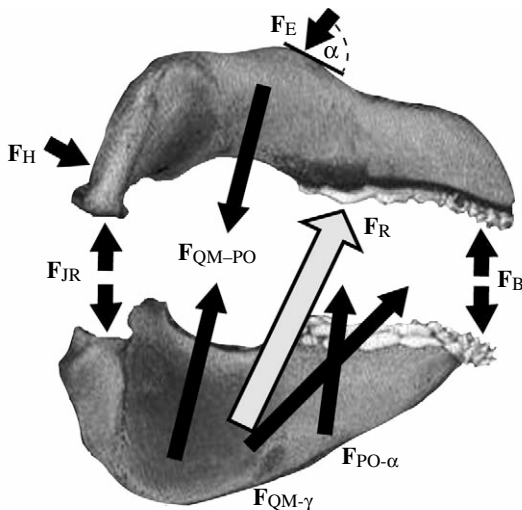

Fig. 4. Forces involved in the static equilibrium calculations of the lower and upper jaws of *H. francisci*. $\mathbf{F}_B$, bite reaction force; $\mathbf{F}_E$, reaction force at the ethmoidal articulation; $\mathbf{F}_H$, reaction force at the hyomandibular articulation; $\mathbf{F}_{JR}$, jaw joint reaction force; $\mathbf{F}_{PO-\alpha}$, force generated by the preorbitalis-α; $\mathbf{F}_{QM-PO}$, force generated by the quadratomandibularis–preorbitalis complex; $\mathbf{F}_{QM-\gamma}$, force generated by the quadratomandibularis-γ; $\mathbf{F}_R$, resultant adductive force; α, angle of incidence of $\mathbf{F}_E$ relative to the articular surface of the upper jaw at the ethmoidal articulation. Arrow size does not indicate force magnitude, and angles of force vectors are approximate. CT-scan image used with permission of A. Summers.

Mathcad 11.1 software (Mathsoft, Inc., Cambridge, MA, USA) was used to generate a three-dimensional model of the static forces acting on the jaws of *H. francisci* during prey capture. Summation of the three-dimensional moments acting on the lower jaw about the jaw joints (left and right) determined the theoretical maximum bite force for each individual and the mean maximum bite force for all individuals ($\bar{F}_B$; Fig. 4). Maximum bite force was modeled at points 0, 25, 50, 75 and 100% of the distance along the functional tooth row from the posteriormost tooth to determine a bite force gradient along the lower jaw. Additionally, the reaction force acting on the jaw joints during bites occurring at 0 and 100% of the distance along the functional tooth row was determined ($\mathbf{F}_{JR}$; Fig. 4).

Loadings were determined at the ethmoidal and hyomandibular articulations of the upper jaw with the chondrocranium and hyomandibula, respectively (Figs 1A, 4). For bites occurring at 0% (posteriormost molariform tooth) and 100% (anteriormost cuspidate tooth) of the distance along the functional tooth row, the moments acting on the upper jaw about the ethmoidal articulation were summed to determine the forces acting at the hyomandibular articulation ($\mathbf{F}_H$; Fig. 4). In these analyses, the hyomandibula was modeled as a two-force member, moveable about its articulations with both the upper jaw and chondrocranium (Hibbeler, 2004). Static equilibrium analysis of the forces acting on the upper jaw was then used to determine the forces acting at the ethmoidal articulation ($\mathbf{F}_E$; Fig. 4). Static equilibrium conditions for the forces acting on the lower ($\mathbf{F}_{LJ}$) and upper jaws ($\mathbf{F}_{UJ}$) were:

$$\Sigma \mathbf{F}_{LJ} = \mathbf{F}_{JR} + \mathbf{F}_{QM-PO} + \mathbf{F}_{QM-\gamma} + \mathbf{F}_{PO-\alpha} + \mathbf{F}_B = 0 , \quad (2)$$

$$\Sigma \mathbf{F}_{UJ} = \mathbf{F}_{JR} + \mathbf{F}_H + \mathbf{F}_{QM-PO} + \mathbf{F}_E + \mathbf{F}_B = 0 , \quad (3)$$

where $\mathbf{F}_B$ is the bite reaction force from a prey item, $\mathbf{F}_{PO-\alpha}$ is the force generated by the preorbitalis-α, $\mathbf{F}_{QM-PO}$ is the force generated by the quadratomandibularis–preorbitalis complex, and $\mathbf{F}_{QM-\gamma}$ is the force generated by the quadratomandibularis-γ. Forces generated by the preorbitalis-α and quadratomandibularis-γ are isolated to the lower jaw because they originate on the chondrocranium and insert only upon the lower jaw (Figs 2A, 4). Joint reaction forces maintain the static equilibrium of feeding mechanisms by balancing the moments acting upon the jaws *via* their associated musculature and contact with prey items. The moment acting on the lower jaw during jaw opening *via* the coracomandibularis muscle was used to determine the theoretical maximum jaw opening force of *H. francisci*.

In situ *bite performance measurements*

Bite performance measurements were performed using a modified single-point load cell (Amcells Corp., Carlsbad, CA, USA) with custom-designed stainless steel lever arms, which was calibrated using a series of known weights. Free-swimming *H. francisci* were trained to voluntarily bite the transducer by wrapping the device with squid and presenting it to them after several days of food deprivation. A P-3500 strain indicator

(Vishay Measurements Group, Raleigh, NC, USA) was used for transducer excitation and signal conditioning. Data were acquired with a 6020E data acquisition board and LabVIEW 6.0 software (National Instruments Corp., Austin, TX, USA). Fifteen measurements of bite force were taken from each animal. Only events in which the transducer was bitten between the tips of the jaws were kept for analysis. The five largest bite force measurements for each individual were analyzed for the following performance variables, as well as used in the multivariate statistical analyses described below: maximum force (N), duration of force production (ms), time to maximum force (ms), rising slope of force–time curve (N s^{-1}), duration at maximum force (ms), time from maximum force to end of force production [hereafter referred to as 'time away from maximum force' (ms)], falling slope of force–time curve (N s^{-1}) and impulse (*I*), which is the integrated area under the force–time curve (kg m s^{-1}) from the initiation of force generation to its cessation:

$$I = \int F \, dt \, , \tag{4}$$

where *F* is force and *t* is time. The impulse of a force is the extent to which that force changes the momentum of another body, in this case the force transducer, and therefore has the units of momentum (kg m s^{-1}). For each individual, the single largest bite force and its associated performance measurements were used to create a profile of maximum bite performance for *H. francisci*, to compare the dynamics of the ascending and descending portions of the bite performance waveforms and to compare the maximum bite forces obtained from the theoretical, *in situ*, restrained and stimulated methods of determining bite force (see below).

In situ bite performance measurements were simultaneously filmed with a Redlake PCI-1000 digital video system (Redlake MASD, San Diego, CA, USA) at 250 frames s^{-1} to verify that bites on the transducer occurred between the tips of the jaws (hereafter referred to as 'transducer bites'). The modified single-point load cell used in this study averages the signals generated by four strain gages in a full Wheatstone bridge such that the transducer is insensitive to the position on the lever arms at which the bite is applied. Therefore, the point at which a shark bit the lever arms of the transducer did not need to be determined from the digital video sequences for appropriate calibration. To identify any behavioral artifacts associated with biting a stainless steel transducer, *H. francisci* were also filmed while consuming pieces of *O. oglinum* cut to the same size as the biting surface of the force transducer (hereafter referred to as 'fish bites'). The following kinematic variables were quantified from transducer and fish bites using Motionscope 2.01 (Redlake MASD, San Diego, CA, USA) and SigmaScan Pro 4.01 software: distance, duration, velocity and acceleration of lower jaw depression, lower jaw elevation, upper jaw protrusion, and head depression; maximum gape; time to maximum gape; time to onset of lower jaw elevation; time to onset of head depression; cranial elevation angle. All kinematic variables were quantified using discrete cranial landmarks as reference points (Edmonds et al., 2001).

Restrained and stimulated bite performance measurements

At least one week after the *in situ* bite performance measurements, four of the *H. francisci* were individually removed from the experimental tank and restrained on a table. Once they had opened their jaws an adequate distance, the transducer was placed between the anterior teeth, which elicited an aggressive bite. Following a recovery period of approximately 10–15 min, the shark was again removed from the tank and anaesthetized with MS-222 (0.133 g l^{-1}). The quadratomandibularis–preorbitalis complex, quadratomandibularis-γ and preorbitalis-α were implanted with stainless steel 23-gauge hypodermic needles connected to a SD9 stimulator (Grass Telefactor, West Warwick, RI, USA), and tetanic fusion of these muscles was accomplished *via* stimulation (10 V, 100 Hz, 0.02 ms delay, 3 ms pulse width) while the bite force transducer was placed between the tips of the anterior teeth. Three measurements were taken from each individual in both of these experimental protocols. Individuals were ventilated with aerated seawater between measurements during muscle stimulation experiments. Maximum bite force, time to maximum force, and time away from maximum force were quantified from all restrained and stimulated bites.

Statistical analysis

All bite performance and kinematic variables were log$_{10}$ transformed and linearly regressed against body mass to remove the effects of size. Studentized residuals were saved from each regression for subsequent analysis (Quinn and Keough, 2002). Principal components analyses (PCA) based on correlation matrices were then used to (1) identify covariation in bite performance variables and reduce these variables to a series of non-correlated principal components, which were subsequently analyzed to assess the extent of individual variability in these parameters, (2) identify covariation in performance and kinematic variables from *in situ* bite performance trials and (3) identify covariation in kinematic variables from fish and transducer bites and reduce these variables to a series of non-correlated principal components, which were subsequently analyzed to determine whether there were any behavioral artifacts associated with biting the steel transducer. Variables were considered to load strongly on a given principal component (PC) if their factor scores were greater than 0.6. Non-rotated axes described the greatest amount of variability in each PCA. For analyses 1 and 3, multivariate analysis of variance (MANOVA) was used to compare the factor scores for the PCs with eigenvalues greater than 1.0. To determine whether fish and transducer bites differed kinematically, a two-way, mixed-model MANOVA was performed on the PCs from PCA 3, with 'individual' as the random effect and 'prey type' as the fixed effect, which was tested over the interaction mean square. Kinematic data from four individuals were included in this analysis because a complete data set was lacking for one individual. To determine the extent of individual variability within the bite performance variables, a one-way MANOVA was performed on the PCs from PCA 1.

To determine whether the kinematic variables associated with biting the transducer were predictive of biting performance in *H. francisci*, stepwise (forward) multiple regressions were performed with kinematic variables measured from transducer bites as the multiple independent factors, and the eight bite performance variables as the individual dependent factors. Data from four individuals were included in this analysis because a complete kinematic data set was lacking for one individual. One-way ANOVA on Studentized residuals was used to identify significant differences among the theoretical, *in situ*, restrained and electrically stimulated methods of determining maximum bite force. A Student's *t*-test was used to identify differences between time to maximum force and time away from maximum force and between the rising and falling slopes of the force–time curves for *in situ* biting trials. One-way ANOVA was used to compare time to maximum force and time away from maximum force within and among *in situ*, restrained and electrically stimulated bite forces. Finally, bite forces at the anterior jaw (fish, reptiles and birds) or canine teeth (mammals) and body masses for various vertebrates were compiled from the available literature and grouped according to major taxonomic level. These bite forces, along with those of the horn sharks investigated in this study, were linearly regressed against body mass. Studentized residuals from this regression were then coded according to taxonomic level and compared with a one-way ANOVA. All significant differences were investigated *post-hoc* with Tukey's pairwise comparisons test. Linear regressions were performed in SigmaStat 2.03 (SYSTAT Software, Inc.) in order to obtain Studentized residuals. All other statistical analyses were performed in SYSTAT 10 (SYSTAT Software, Inc.) with a *P*-value of 0.05.

Results

Biomechanical modeling

The quadratomandibularis–preorbitalis complex, which is the primary jaw adductor, generated the greatest force of all muscles investigated (242 N; Table 1). Of the muscles active during jaw and hyobranchial abduction, the coracobranchiales generated the greatest force (107 N; Table 1). The levator hyomandibularis generated more force during the retractive phase (33 N) than the levator palatoquadrati (20 N; Table 1). After resolving the force generated by the adductor musculature into its principal components, the majority of force was directed dorsally (294 N) and anteriorly (128 N). The Z-axis components of this force (19 N per side) were directed laterally on either side of the head and negate each other during jaw adduction (Table 2; Fig. 3A). Thus, the resultant adductive force along the Z-axis was 0 N. The large anterodorsally directed component of this adductive bite force ($\mathbf{F_R}$; Fig. 4) drives the lower jaw towards the upper jaw, which is itself driven into the ethmoid region of the chondrocranium ($\mathbf{F_E}$; Fig. 4).

Table 1. *Theoretical maximum forces generated by the cranial musculature active during the gape cycle in* H. francisci

Action	Muscle	Theoretical maximum force (N)
Jaw and hyobranchial abduction	Coracomandibularis	31±5
	Coracohyoideus	57±4
	Coracoarcualis	87±4*
	Coracobranchiales	107±8*
Jaw adduction	Quadratomandibularis-γ	44±2*
	Preorbitalis-α	52±5*
	QM–PO complex	242±11*
Jaw and hyobranchial retraction	Levator palatoquadrati	20±1*
	Levator hyomandibularis	33±1*

Values are means ± S.E.M.
*Bilateral muscle force for paired muscles.

Table 2. *Resultant bilateral muscle and jaw forces occurring during prey capture in* H. francisci, *broken into their principal components*

Variable	Resultant force (N)	$\mathbf{F_X}$ (N)	$\mathbf{F_Y}$ (N)	$\mathbf{F_Z}$ (N)
Resultant abductive muscle force	31	25	–19*	0
Resultant adductive muscle force	321	–128*	294	0
Opening force†	16	0	–16*	0
Biting force† ($\mathbf{F_B}$)	128	0	128	0
Biting force‡ ($\mathbf{F_B}$)	338	0	338	0

*Negative values indicate forces acting in the negative direction on their respective axes (see Fig. 2A).
†Force at the tips of the jaws.
‡Force at the back of the jaws.

Summation of the moments acting on the lower jaw determined that the maximum theoretical bite force of *H. francisci* ranged from 128 N at the anterior teeth to 338 N at the posteriormost molariform teeth (Fig. 5; Table 2). The bite force at the posteriormost molariform teeth exceeded the resultant force generated by the adductive musculature (Table 2) because the mechanical advantage at this point along the jaw was 1.06. The resultant jaw closing mechanical advantage at the anterior teeth was 0.51, resulting in a dramatically lower bite force at this point.

The jaw joint reaction forces (F_{JR}; Fig. 4) occurring when prey is captured at the anterior teeth and crushed at the posterior teeth by *H. francisci* were 106 N and 73 N per side, respectively (Table 3). This force was oriented posteroventrally relative to the articular surface of the lower jaw joint for anterior biting, and consequently oriented anterodorsally relative to the articular surface of the upper jaw joint. The local/internal loadings on the joint between the upper and lower jaws indicate that the jaw joint is globally in *compression* (Hibbeler, 2004) when prey is bitten at the tips of the jaws. When prey is crushed between the posterior molariform teeth, the orientation of the vertical component of
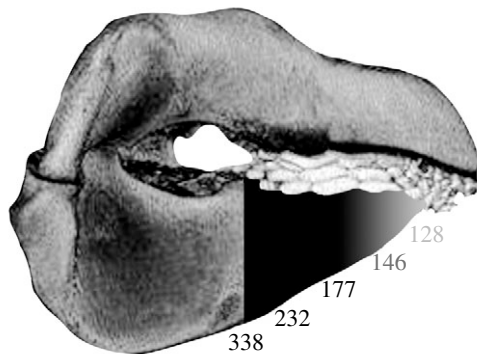

Fig. 5. Theoretical maximum bite force (N) of five male *H. francisci* (*N*=5, *TL*=55–68 cm) from three-dimensional vector analysis of the jaw adducting musculature measured at 0, 25, 50, 75 and 100% of the length of the functional tooth row of the lower jaw from posterior to anterior. CT-scan image used with permission of A. Summers.

the joint reaction force relative to the lower jaw (25 N) was opposite that for the lower jaw joint during anterior biting (–80 N), indicating *tensile* loading of the jaw joint during posterior prey capture (Table 3).

The ethmoidal articulation of *H. francisci* received a loading of 59 N per side during biting, regardless of whether biting occurred at the anterior or posterior margin of the jaws (F_E; Fig. 4). The angle of incidence of this force relative to the articular surface of the upper jaw at the ethmoidal articulation was 80° (α; Fig. 4). For both anterior and posterior biting, the majority of loading was directed ventrally into the upper jaw, indicating *compression* between the ethmoid region of the chondrocranium and the palatal region of the upper jaw (Table 3).

The magnitude of loading at the hyomandibular articulation (36 N) was independent of bite point as well (F_H; Fig. 4). The lower jaw was loaded posterodorsally and medially at its articulation with the hyomandibula during both anterior and posterior biting (Table 3). The reaction forces acting on the distal ends of the hyomandibula are equal to and opposite the forces acting at the jaws' articulation with the hyomandibula. Therefore, during biting, the hyomandibula was loaded anteroventrally and laterally. These local/internal loadings between the jaws and hyomandibula indicate that the hyomandibula is globally in *tension*. Modeling the hyomandibula as a two-force member assumed that the line of action of the force acting on the hyomandibula passed through its articulation with the jaws and chondrocranium. The hyomandibula is therefore loaded in pure tension, and the angle of incidence of the hyomandibular force cannot be determined.

The only muscle involved in abduction of the lower jaw is the coracomandibularis, which was capable of generating 31 N of force (Table 1). This muscle inserts on the caudal aspect of the lower jaw symphysis at 37° below the longitudinal axis of this jaw and has a mechanical advantage of 0.89. Despite this high mechanical advantage, indicative of force amplification in a class III lever system, its acute insertion angle caused the muscular force generating motion about the lower jaw (force component perpendicular to the lower jaw) to be 19 N

Table 3. *Unilateral mechanical loadings at articulation points in* H. francisci*'s feeding mechanism, broken into their principal components*

Variable	Resultant force (N)	F_X (N)	F_Y (N)	F_Z (N)
Joint reaction force[†] (F_{JR})	106	69	–80*	0
Joint reaction force[‡] (F_{JR})	73	69	25	0
Loading at ethmoidal artic.[†] (F_E)	59	10	–59*	0
Loading at ethmoidal artic.[‡] (F_E)	59	10	–59*	0
Loading at hyomandibular artic.[†] (F_H)	36	10	22	27
Loading at hyomandibular artic.[‡] (F_H)	36	10	22	27

*Negative values indicate forces acting in the negative direction on their respective axes relative to the right side of *H. francisci*'s head (see Fig. 2A). Artic, articulation.

[†]Force at the tips of the jaws.

[‡]Force at the back of the jaws.

(Table 2). After accounting for mechanical advantage, the resultant abductive force at the tip of the lower jaw was 16 N (Table 2). The abductive force lacks a component along the *Z*-axis because the coracomandibularis runs parallel to the longitudinal axis of the body. The other muscles involved in the expansive phase of the gape cycle generated considerably greater forces than the coracomandibularis (Table 1).

Performance measurements

In situ *measurements*

H. francisci approached and bit the force transducer in an attempt to remove the attached food. In most cases, biting continued until the food was removed from the transducer. PCA 1 reduced the performance variables for each individual to three PCs (89.7% of variance explained), each of which indicated considerable overlap among individuals. MANOVA subsequently demonstrated no differences among individuals for bite performance variables using size-corrected data (Wilk's Lambda=0.51, $F_{12,47}$=1.157, P=0.340). The mean maximum *in situ* bite force measured at the anterior teeth was 95 N, with an absolute maximum force of 133 N (66 cm male *H. francisci*). *Heterodontus francisci* took approximately 322 ms to reach maximum bite force, which was held for 41 ms, and released after an additional 212 ms (Table 4). The mean duration of force application was 535 ms. Time to maximum bite force was longer than the time away from maximum bite force (P=0.049). The mean rising slope of the force–time curve was 300 N s^{-1} and was lower than the mean falling slope of 457 N s^{-1} (P=0.048). The mean impulse generated from the beginning of force application until its cessation was 25 kg m s^{-1} but measured as high as 44 kg m s^{-1}. The majority of bite force waveforms consisted of single peaks associated with single bites. However, in 32% of the bites, multiple peaks occurred, indicating a repetitive crushing behavior during force application (Fig. 6).

PCA 2 of performance and kinematic variables yielded six PCs with eigenvalues greater than 1.0, which collectively explained 86.7% of the variance. All of the variables that loaded heavily on the first PC (30.5% of variance explained) were kinematic measurements (Table 5). These variables primarily demonstrated covariance in the timings and excursions of lower jaw depression and elevation. Performance measures were the only variables to load heavily on the second
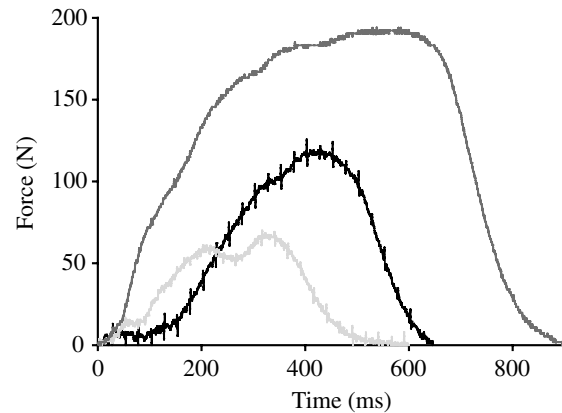

Fig. 6. Bite force waveforms from bite performance trials of three male *H. francisci* (*TL*=66–70 cm), illustrating *in situ* voluntary bites with single (black) and double (light gray) force peaks and a bite from a restrained individual (dark gray).

PC (19.5% of variance explained), indicating covariance between rates and durations of force application (Table 5). Maximum bite force did not load heavily until the fifth PC (7.8% of variance explained), and impulse did not load heavily on any of the PCs.

Stepwise multiple regressions yielded similar results to PCA 2 on kinematic and performance data. Only three of the bite performance variables were significantly related to individual kinematic variables. Force duration was significantly, though poorly, related to lower jaw elevation velocity (r^2=0.226, $F_{1,18}$=5.268, P=0.034). Similarly, time to maximum force (r^2=0.389, $F_{1,18}$=11.471, P=0.003) and the rising slope of the force–time curve (r^2=0.410, $F_{1,18}$=12.523, P=0.002) were significantly related to lower jaw elevation distance. Inclusion of additional kinematic variables did not improve the predictive ability of these regression models. The two variables indicative of the magnitude of bite force generated (maximum force, impulse) could not accurately be predicted by any combination of kinematic variables. Although kinematic variables were not predictive of bite performance variables, PCA 1 used to assess individual variability (see above) identified notable covariance in performance measures. Maximum *in situ* bite force exhibited a strong linear relationship with impulse (r^2=0.758) and moderate linear

Table 4. In situ *bite performance data for* H. francisci *biting at the tips of its jaws*

Variable	Minimum	Maximum	Mean ± S.E.M.
Maximum force (N)	60	133	95±13
Force duration (ms)	400	721	535±60
Time to maximum force (ms)	241	428	322±33
Time at maximum force (ms)	31	55	41±4
Time away from maximum force (ms)	146	303	212±35
Impulse (kg m s^{-1})	11	44	25±6
Rising slope of force–time curve (N s^{-1})	200	400	300±34
Falling slope of force–time curve (N s^{-1})	305	696	457±65

Table 5. *Principal component loadings of performance and kinematic variables from bite performance trials of H. francisci*

Variable	PC 1	PC 2
Lower jaw depression distance	**0.718**	0.179
Lower jaw depression duration	**0.820**	0.066
Lower jaw depression velocity	0.122	0.183
Lower jaw depression acceleration	–0.378	0.199
Time to maximum gape	**0.741**	0.182
Maximum gape	0.496	0.467
Head angle	0.403	0.334
Onset of lower jaw elevation	**0.830**	0.015
Lower jaw elevation distance	**0.727**	0.219
Lower jaw elevation duration	0.459	0.530
Lower jaw elevation velocity	–0.533	0.352
Lower jaw elevation acceleration	**–0.710**	–0.001
Time to lower jaw elevation	**0.939**	0.098
Time to maximum force	–0.051	**–0.772**
Time at maximum force	0.325	**–0.704**
Time away from maximum force	0.593	–0.475
Force duration	0.326	**–0.829**
Rising slope	0.152	**0.800**
Falling slope	–0.457	**0.643**
Impulse	0.460	–0.127
Maximum force	0.069	0.305

Bold values indicate variables considered to load heavily on a given principal component (loading score >0.600).

Fig. 7. Maximum *in situ* bite force (N) from five male *H. francisci* (*TL*=63–74 cm) plotted against (A) impulse (kg m s^{-1}) and (B) force duration (ms) on logarithmic axes.

relationships with force duration (r^2=0.450) (Fig. 7) and time to maximum force (r^2=0.489).

PCA 3 reduced the set of kinematic variables measured from fish and transducer bites to a series of four PCs (73.3% of variance explained). MANOVA indicated no significant differences between the prey capture kinematics of *H. francisci* while biting fish or the transducer on any of the PCs for all individuals (Wilk's Lambda=1.0, $F_{4,29}$=0.0, P=1.0). However, a single individual was found to differ from two other individuals on the first PC ($F_{3,32}$=4.646, P=0.008). Variables that loaded heavily on the first PC were durations and distances of lower jaw depression and elevation, times to maximum gape, onset of lower jaw elevation, completion of lower jaw elevation and maximum gape distance. The acceleration of lower jaw elevation loaded heavily, but negatively, on the first PC.

Methodological comparison

In situ measurement of maximum bite force was a reasonably good indicator of the maximum bite force of *H. francisci*. Using size-corrected data, a single difference was found among the four methods of determining maximum bite force ($F_{3,14}$=4.358, P=0.023). Restrained bite force (159–206 N) was significantly greater than *in situ* bite force (60–133 N) (P=0.013). *In situ* bite force was, however, equivalent to theoretical (107–163 N) and electrically stimulated (62–189 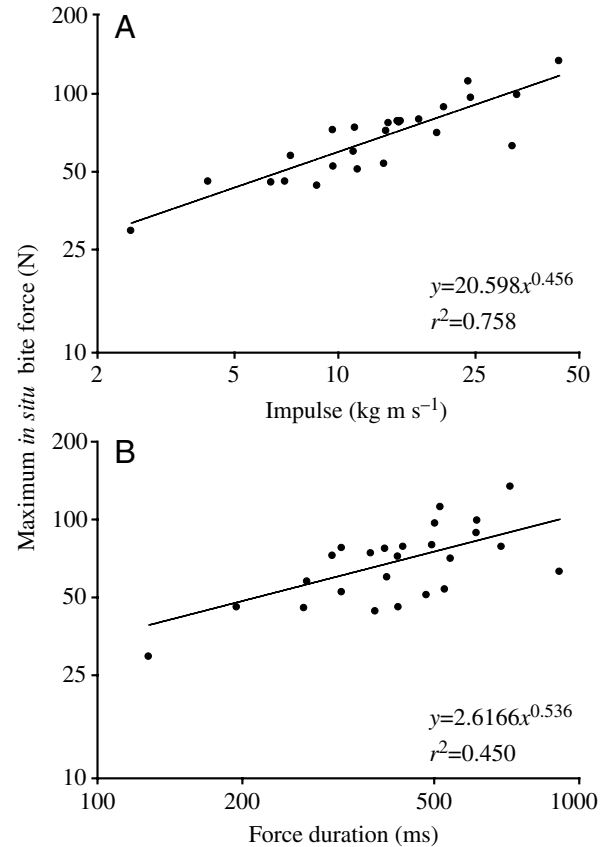N) bite forces. Restrained, electrically stimulated and theoretical bite forces were equivalent (Table 6). During restrained bites, time to maximum force (522 ms) was greater than time away from maximum force (339 ms) (t_4=2.848, P=0.046). Time to maximum force (285 ms) was shorter than time away from maximum force (556 ms) for electrically stimulated bites (t_8=–5.476, P<0.001). Significant differences were detected between the *in situ*, restrained and electrically stimulated methods for time to maximum force ($F_{2,10}$=4.996, P=0.031) and time away from maximum force ($F_{2,10}$=58.290, P<0.001). Time to maximum force was greater for restrained bites than for electrically stimulated bites (P=0.030), both of which were equivalent to the time to maximum force of *in situ* bites. Time away from maximum force was greater for electrically stimulated bites than restrained bites (P=0.001), which was greater than that of *in situ* bites (P=0.005).

Bite forces among vertebrates

Bite forces and body masses were compiled for 113 species of vertebrates (including *H. francisci*) from the available literature (Binder and Van Valkenburgh, 2000; Cleuren et al., 1995; Clifton and Motta, 1998; Erickson et al., 2004; Hernandez and Motta, 1997; Herrel et al., 1999, 2001, 2002; Huber et al., 2004; Huber and Motta, 2004; Korff and

Table 6. *Results of one-way ANOVA on different methods of determining bite force at the tips of the jaws in* H. francisci

	In situ	Theoretical	Stimulated	Restrained
Mean max. ± S.E.M. (N)	95±13[a]	128±10[a,b]	132±24[a,b]	187±14[b]

Statistically similar values are represented by the same lower-case letters. Values are the means of the single largest bite force values from each individual.

Wainwright, 2004; Ringqvist, 1972; Robins, 1977; Thomason et al., 1990; Thompson et al., 2003; van der Meij and Bout, 2004; Weggelaar et al., 2004; Wroe et al., 2005; D. R. Huber, M. N. Dean, and A. P. Summers, unpublished) (Appendix I). Collectively, bite force scaled to body mass with a coefficient of 0.60, which is below the isometric scaling coefficient of 0.67 (Fig. 8). When the mammalian bite forces from Wroe et al. (2005) were excluded from this analysis, bite force scaled with a coefficient of 0.66, approximating isometry. This discrepancy is probably due to Wroe et al. (2005) having used the dry-skull method of estimating muscle A_{cs}, which can underestimate A_{cs} by 1.3–1.5× (Thomason et al., 1991).

Fishes collectively had the highest mass-specific bite force of the four vertebrate groups, followed by reptiles, mammals

and birds, respectively ($F_{3,130}$=6.357, $P<0.001$). Mass-specific bite force of the fishes was greater than those of the birds ($P=0.002$) and mammals ($P=0.013$), while reptilian mass-specific bite force was greater than that of the birds ($P=0.009$). The striped burrfish, *Chilomycterus schoepfi*, had the highest mass-specific bite force, followed by the Canary Island lizard, *Gallottia galloti*, and the American alligator, *Alligator mississippiensis* (Erickson et al., 2004; Herrel et al., 1999; Korff and Wainwright, 2004). The hogfish, *Lachnolaimus maximus*, had the second highest mass-specific bite force, but for biting with the pharyngeal jaws not the oral jaws (Clifton and Motta, 1998). The three lowest mass-specific bite forces were those of the red-bellied short-necked turtle, *Emydura subglobosa*, the mata mata turtle, *Chelus fimbriatus*, and the twist-necked turtle *Platemys platycephala* (Herrel et al., 2002) (Fig. 8). Of the cartilaginous fishes in this analysis, the mean mass-specific bite force of *H. francisci* was greater than those of *S. acanthias* and the blacktip shark, *Carcharhinus limbatus*, but less than that of the white-spotted ratfish, *Hydrolagus colliei*.

Discussion

Functional morphology

The jaw adducting cranial musculature (QM–PO complex, QM-γ, PO-α on Fig. 2) of *H. francisci* generates more force during prey capture than either the jaw and hyobranchial abducting or retracting musculature. The mechanical advantage of *H. francisci*'s jaw adducting mechanisms ranges from 0.51 at the tip of the jaws to 1.06 at the posterior margin of the functional tooth row. In class III lever systems such as shark jaws, a mechanical advantage greater than 1.0 indicates that the point at which force is being applied to a prey item is closer to the jaw joint than the point at which muscular force is being applied to the jaw, resulting in an amplification of the muscular force. Subsequently, the theoretical maximum bite force at the posterior margin of the functional tooth row exceeds the resultant force generated by *H. francisci*'s adductor musculature. This amplification of muscular force is advantageous for the processing of hard prey such as the molluscs, echinoderms and benthic crustaceans consumed by *H. francisci* (Segura-Zarzosa et al., 1997; Strong, 1989).

The jaw closing mechanical advantage at the anterior teeth of *H. francisci* is greater than that of the only other elasmobranch for which values have been published, *S. acanthias* (0.28; Huber and Motta, 2004), which utilizes a combination of ram and suction feeding to consume soft-
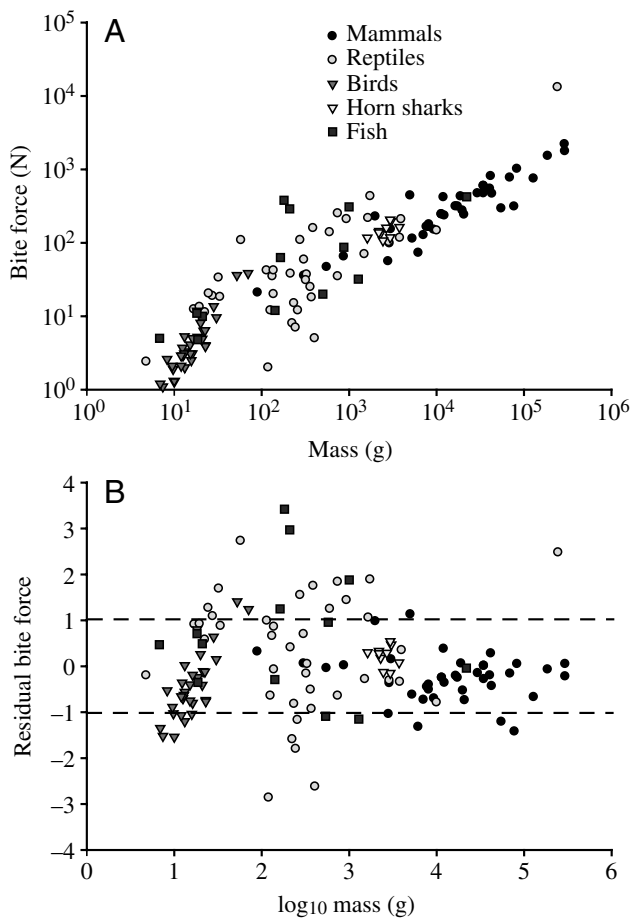

Fig. 8. (A) Bite forces (N) of various vertebrates plotted against mass (g). (B) Residuals from regression analysis of $\log_{10}$ bite force *versus* $\log_{10}$ mass plotted against $\log_{10}$ mass (g). Broken lines indicate ± 1 standard deviation about the residual mean.

bodied prey (Wilga and Motta, 1998). Its jaw closing mechanical advantage is greater than those at the anterior teeth of nearly every actinopterygian fish investigated (~150), which include prey from plankton to hard-shelled species (Durie and Turingan, 2001; Turingan et al., 1995; Wainwright et al., 2004; Westneat, 2004). The durophagous species among these taxa do, however, have the highest jaw adducting mechanical advantages. The durophagous parrot fishes (Scaridae) are the only actinopterygian fishes with jaw adducting mechanical advantages comparable with that of *H. francisci* (Wainwright et al., 2004; Westneat, 2004). Thus, there is extensive evolutionary convergence on high leverage jaw adducting mechanisms in fishes that consume hard prey.

The jaws of *H. francisci* are elliptical in transverse-section, with their major axis oriented vertically, in-line with the compressive stresses associated with feeding. Calcium reinforcement in the jaw cortex increases posteriorly as the dentition becomes more molariform and is greatest at the jaw joints (Summers et al., 2004). Calcification and elliptical geometry increase the second moment of area of the jaws with respect to the compressive loading of prey capture and processing, which augments the jaws' ability to resist dorsoventral flexion (Summers et al., 2004). The resolved force vector for jaw adduction also occurs approximately in the region of the most robust molariform teeth of *H. francisci*, where it can generate upwards of 338 N of bite force. Therefore, maximum bite force is produced where both the dentition and jaw cartilages are best able to resist compressive stresses.

Despite the high mechanical advantage (0.89) of the coracomandibularis muscle in the lower jaw depression mechanism of *H. francisci*, its acute insertion angle relative to the lower jaw causes most of its force to be directed posteriorly, into the jaw joints (Table 2.) This high mechanical advantage is due to the insertion of the coracomandibularis on the posterior margin of the mandibular symphysis, which is synapomorphic for elasmobranchs (Wilga et al., 2000). Although this mechanism is suited for force production, velocity production is desirable for inertial suction feeding. *Heterodontus francisci* nonetheless effectively uses suction to initially capture and reorient prey (Edmonds et al., 2001), which may be due in part to its powerful hyoid and branchial abductors (Table 1). These muscles rapidly expand the floor of the buccopharyngeal cavity, which is critical to suction feeding in elasmobranchs (Motta et al., 2002; Svanback et al., 2002). As in the nurse shark, *Ginglymostoma cirratum* (Motta et al., 2002), the large labial cartilages of *H. francisci* considerably occlude its lateral gape, theoretically augmenting suction ability (Muller and Osse, 1984; Van Leeuwen and Muller, 1984).

Three-dimensional resolution of the forces generated during jaw adduction may reveal the mechanical basis of upper jaw protrusion in *H. francisci*. The force driving the upper jaw into the ethmoidal articulation has both dorsal and anterior components, causing the upper jaw to slide through the anteroventrally sloping palatal fossa of the chondrocranium

and protrude (Fig. 4; Table 2). This proposed mechanism is based on the resolved force vector for all muscles involved in jaw adduction. Differential activity of the heads of this complex may facilitate modulation of protrusion. The quadratomandibularis-γ is the likely candidate for control over protrusion because its acute insertion angle relative to the lower jaw and anterior insertion point give it high leverage over anterior motion (Fig. 2).

Activity of the quadratomandibularis–preorbitalis complex alone, which has a broad insertion on the lateral face of both the upper and lower jaws, may contribute to protrusion of the upper jaw as well. After the lower jaw has been depressed, contraction of this muscle complex may simultaneously raise the lower jaw and pull the upper jaw away from the skull. This mechanism has been proposed for upper jaw protrusion in *S. acanthias*, *G. cirratum* and the lemon shark, *Negaprion brevirostris* (Moss, 1977; Motta et al., 1997; Wilga and Motta, 1998). Protrusion by *H. francisci*, which may be used to chisel away at attached benthic prey, occurs after the lower jaw has been depressed (Edmonds et al., 2001), corroborating the role of the quadratomandibularis–preorbitalis complex in this behavior.

Extensive calcification near the jaw joints of *H. francisci* (Summers et al., 2004) would apparently indicate high joint reaction forces during prey capture. Joint reaction forces can exceed bite forces at the tip of the jaw depending on the mechanical advantage of the given feeding mechanism and the force produced by the associated musculature, which has been identified in numerous reptiles (3–4× greater; Cleuren et al., 1995; Herrel et al., 1998). Although joint reaction force was greater than anterior bite force in *H. francisci*, the ratio of these values (1.65) is substantially lower than those found for reptiles. The ratio of joint reaction force to posterior bite force in *H. francisci* was 0.43.

Low ratios of joint reaction force to bite force in *H. francisci* are due to its high mechanical advantage jaw adducting mechanism. Humans, which share this characteristic, have correspondingly low ratios of joint reaction force to bite force (Koolstra et al., 1988). Although some damping will occur in the connective tissue associated with the jaw joint, loading occurring at the joint will be transmitted to adjacent skeletal elements. Therefore, low ratios of joint reaction force to bite force may be adaptive in *H. francisci*, and elasmobranchs in general, because the posterior region of their jaws is suspended from the cranium by mobile hyomandibulae, not a stable jaw articulation as in other vertebrates. Minimizing loading at this articulation may stabilize the feeding mechanism during prey capture and processing.

In heterodontiform sharks, the cranial stresses associated with prey capture can be isolated to the ethmoidal and hyomandibular articulations. Unlike carcharhinid sharks (Motta and Wilga, 1995), the upper jaw of *H. francisci* does not disarticulate from the chondrocranium during feeding, even during upper jaw protrusion (Maisey, 1980). Therefore, in carcharhinid sharks, the hyomandibulae may receive all of the suspensorial loading occurring during prey capture. Optimal

loading at the ethmoidal articulation would entail forces directed perpendicularly into the articular surface of the upper jaw because cartilage is strongest in axial compression (Carter and Wong, 2003). The estimated forces at this articulation deviated from optimal orientation by only 10° during anterior and posterior biting. The ethmoidal articulation of *H. francisci* appears well designed for withstanding this nearly axial compressive loading because the upper jaw calcifies at this articulation early in ontogeny (Summers et al., 2004) and the ethmoid region of the chondrocranium is one of the thickest parts of this structure (Daniel, 1915). Additionally, maintenance of contact between the upper jaw and chondrocranium in *H. francisci* will distribute stresses from the repetitive loading associated with processing hard prey.

Although it is well known that the hyomandibulae support the posterior margin of the jaws, the nature of the loading they receive has been a matter of speculation. This mechanical analysis indicates that the hyomandibulae of *H. francisci* are tensile elements, as suggested by Moss (1972) and Frazzetta (1994). Consequently, the hyomandibulae may regulate anterior movement of the jaws during feeding, such as would occur during jaw protrusion. In this regulatory role, activity of the levator hyomandibularis could hypothetically modulate resistance to anterior motion of the jaws. Electromyographic analysis of the feeding musculature of *H. francisci* would be required to verify this hypothesis.

The ligamentous attachments between the hyoid arch and the posterior end of the jaws stabilize this articulation against the tensile stresses caused by biting. The internal hyomandibular palatoquadrate and hyoideo-mandibulare ligaments resist dorsoventral translation between the hyomandibula and jaws, while the hyomandibuloceratohyal ligament prevents lateral translation between these elements. The two slips of the median ligament (Daniel, 1915) stabilize against dorsoventral and lateral translation, respectively. Although this analysis makes the assumption that the hyomandibulae are loaded as two-force members in axial tension, they probably experience a more diverse loading pattern in nature, necessitating this multidirectional support.

Increased hyomandibular loading may have played a role in the transition from amphistylic to hyostylic jaw suspensions in modern elasmobranchs. As the number and size of the articulations between the jaws and chondrocranium was reduced, the hyomandibulae took on a greater role in suspending the jaws (Carroll, 1988; Maisey, 1980; Schaeffer, 1967). Concomitant with these changes in articulation, the hyomandibulae became shorter and more mobile (Cappetta, 1987; Maisey, 1985; Moy-Thomas and Miles, 1971; Schaeffer, 1967), oriented more orthogonally to the chondrocranium (Stahl, 1988; Wilga, 2002) and had more extensive ligamentous attachments with the jaws and chondrocranium (Gadow, 1888). Collectively, these changes may have been associated with a shifting of the force of jaw adduction to a more posterior region of the jaws. This may have resulted in greater hyomandibular loading as well as a 'freeing-up' of the anterior margin of the jaws such that upper jaw kinesis was

increased, facilitating jaw protrusion and prey gouging (Maisey, 1980; Moss, 1977; Wilga, 2002).

Although the jaw suspension mechanism of *H. francisci* is classified as hyostylic (Gregory, 1904; Wilga, 2002), this analysis indicates that it is functionally amphistylic. *Heterodontus francisci* exhibits considerable upper jaw kinesis (reduces maximum gape by 39%), similar to other hyostylic carcharhiniform sharks (Edmonds et al., 2001; Wilga et al., 2001). Despite this functional similarity, the upper jaw does not disarticulate from the chondrocranium during protrusion in *H. francisci*. Furthermore, in contrast to the hypotheses regarding hyomandibular evolution (see above), *H. francisci* has considerable loading at both the hyomandibular (tensile) and ethmoidal (compressive) articulations. The term 'hyostyly' should therefore be reserved for taxa in which the upper jaw disarticulates from the chondrocranium during protrusion such that hyomandibulae are the primary means of support and the ethmopalatine ligaments are loaded in tension. Therefore, contemporary definitions of jaw suspension should incorporate functional interpretations of loadings at the various articulations between the jaws and cranium, as well as the relationship between suspension type and upper jaw protrusion.

Methodological comparison

Although no differences were found between theoretical, restrained and electrically stimulated bite force measurements using size-corrected data, the absolute maximum bite force for each individual occurred during restrained bite force measurements. No differences were found between theoretical and electrically stimulated bite force measurements of *S. acanthias* either (Huber and Motta, 2004). Therefore, restrained measurements appear to be the best method of obtaining maximum bite force measurements from live elasmobranchs. Small sample size might, however, account for the lack of statistical significance found between different methods of determining bite force. Nonetheless, the results of both this analysis and that of bite force production in *S. acanthias* (Huber and Motta, 2004) indicate that theoretical estimates of bite force in sharks are accurate in predicting maximum bite forces. This is fortunate given the logistical problems associated with obtaining bite force measurements from live elasmobranchs. Given the appropriate resources, however, maximum bite force can be obtained through *in situ* methods, as indicated by the equivalence of theoretical, electrically stimulated and *in situ* bite forces in this study. *In situ* measurements enable the quantification of biting dynamics as well, which is informative regarding feeding performance and ecology (see below).

Static estimates of force production based on muscle architecture may underestimate actual force production because active stretching of the jaw adductors during the expansive phase of the gape cycle can increase force production (Askew and Marsh, 1997; Josephson, 1999). Furthermore, by modeling the primary jaw adductor as the quadratomandibularis–preorbitalis complex instead of

delineating the individual heads of this complex, variations in muscle architecture of these heads such as pinnate insertion points may have been overlooked. If this were the case, a theoretical model of force production based on morphological cross-sectional area alone could underestimate maximum force production.

The ratios of time to and away from maximum force for *in situ* (1.52) and restrained (1.54) bites suggest that the application of bite force by *H. francisci* takes longer than its release. However, the opposite relationship for these variables occurred during electrically stimulated bites. The ratio of time to and away from maximum force during electrically stimulated biting (0.51) approximates the ratio of time for twitch tension development to relaxation (0.42) for pectoral fin muscle of the cuckoo ray, *Raja naevus* (Johnston, 1980). This suggests that force generation during voluntary or stimulated biting is a function of the rate at which the adductor muscles reach tetanic fusion. Gradual summation of motor unit recruitment during voluntary biting results in a prolonged time to maximum force, whereas manual, high-frequency electrical stimulation of the adductor muscles causes more rapid tetani and subsequently shorter times to maximum force. Time away from maximum force was longer for restrained measurements than for *in situ* measurements, perhaps indicating motivational differences between these two presentation methods.

Feeding performance

Several bite performance variables demonstrated patterns consistent with the durophagous diet of *H. francisci*. The time to maximum bite force application by *H. francisci* was longer than time away from maximum force, the rising slope of the force–time curve was lower than the falling slope, and maximum bite force was positively related to the time to maximum force. These performance characteristics indicate that the application of bite force is a slower, more deliberate action than its release by *H. francisci*. Linear relationships of maximum bite force with impulse and force duration further indicate that higher bite forces are associated with slower, more deliberate closing of the jaws by *H. francisci* (Fig. 7).

The impulse generated upon impact between two bodies is a measure of momentum transfer and can be interpreted as the 'effort' that each body exerts on the other (Nauwelaerts and Aerts, 2003). Because momentum is conserved during impact, larger impulses generated during biting transfer greater quantities of kinetic energy from the jaws to the prey. Optimizing impulse by maximizing bite force output per unit time will increase the amount of energy contributing to the rupture/fracture of a prey item. *Heterodontus francisci* capitalizes upon this when consuming hard prey with composite exoskeletons. Sustained loading after a high-velocity initial impact is effective at fracturing composite structures such as sea urchin exoskeletons (calcite ossicles linked by collagenous ligaments) because composites harden to a saturation point upon initial compression, after which crack nucleation occurs, followed by structural failure

(Christoforou et al., 1989; Ellers et al., 1998; Provan and Zhai, 1985; Strong, 1989).

The prevalence of multiple force peaks within a compressive waveform of a single bite (32% of *in situ* bites) also indicates *H. francisci*'s behavioral specialization for exploiting hard prey (Fig. 6). This behavior maximizes the damage inflicted upon prey items during a given bite by ramping up the applied force multiple times, especially when there are multiple bites during a feeding event. The rate at which the strength of a composite structure degrades is a power function of both the strain rate and number of strain cycles (Hwang and Han, 1989). Multiple force peaks within a given bite indicate that *H. francisci* may have evolved motor patterns specialized for durophagy as well. High-frequency bursts of electrical activity associated with rhythmic compression of prey items occur in the jaw adductor musculature of the lungfish *Lepidosiren paradoxa* (Bemis and Lauder, 1986). Prolonged jaw adductor activity occurs in the queen triggerfish, *Balistes vetula* (Turingan and Wainwright, 1993), and the bonnethead shark, *Sphyrna tiburo*, which also uses repeated compressions of the jaws to process prey (Wilga and Motta, 2000). All of these fish include hard prey in their diets (Berra, 2001; Turingan and Wainwright, 1993; Wilga and Motta, 2000). These behavioral attributes demonstrate that the way in which force is applied to prey items, and not just the magnitude of force, is likely to be a determinant of feeding success.

Although covariation in several performance measures appears related to the consumption of hard prey by *H. francisci*, covariation was lacking between kinematic and performance variables from the *in situ* bite performance trials. Both principal components and multiple regression analyses demonstrated the inability of kinematic measures to predict bite performance measures with any accuracy (Table 5). These findings beg the question, how are two series of sequential behaviors so unrelated? One would assume that at least the kinematics of lower jaw elevation (e.g. velocity, acceleration) would be predictive of biting performance (e.g. maximum force, impulse). This lack of covariation is probably due to the instantaneous position of the jaw adducting muscles of *H. francisci* on the force–velocity curve relating muscle tension to contraction velocity (Aidley, 1998). Based on this principle, when the adductor musculature is elevating the lower jaw, it is contracting with high velocity and low force. However, once contact is made with the bite force transducer, movement of the lower jaw is impeded and the jaw adductors shift to the low-velocity, high-force region of the force–velocity curve. In addition to high force, maximum muscle power is generated at low velocity as well (Askew and Marsh, 1997). Because of the dramatic differences in muscle function at either end of the force–velocity curve, jaw kinematics and biting performance may vary conversely and possibly be modulated independently. A predictive relationship between cranial kinesis and performance kinetics is more likely to be found for behaviors such as suction feeding in which kinesis and performance occur simultaneously (cranial expansion and suction generation; Sanford and Wainwright, 2002; Svanback

et al., 2002), not sequentially, as is the case in biting performance (jaw adduction and bite force application).

An additional behavior that may augment the biting performance of *H. francisci* is the use of upper jaw protrusion to dislodge and chisel away at hard prey, as was suggested by Edmonds et al. (2001). While the restrained bite force measurements of *H. francisci* indicate that they can consume prey capable of resisting over 200 N using this behavior, *in situ* bite force measurements suggest they would consume smaller, less durable prey. An analysis of the forces necessary to crush various sizes of hard prey items found in *H. francisci*'s diet is needed to delineate the prey it is theoretically capable of consuming (potential niche) from that which it actually consumes (realized niche). Functioning at maximum capacity would typically be an unnecessary expenditure of energy, especially when feeding occurs in a niche such as durophagy that is relatively inaccessible to sympatric taxa.

Feeding ecology

The cranial architecture and prey capture behavior of *H. francisci* enable it to exploit hard prey, which is a relatively untapped ecological niche for aquatic vertebrates. In fishes, durophagy has been associated with high bite forces and low dietary diversity (Clifton and Motta, 1998; Wainwright, 1988). Species capable of consuming hard prey are morphologically segregated by relative differences in bite force and ecologically segregated by the hardness of the prey they can consume (Aguirre et al., 2003; Kiltie, 1982). Therefore, durophagy appears to result in niche specialization and competition reduction. This is the case in *H. francisci* because hard prey (molluscs, echinoderms, benthic crustaceans) comprises approximately 95% of its diet (Segura-Zarzosa et al., 1997; Strong, 1989). However, Summers et al. (2004) suggested that *H. francisci* goes through an ontogenetic shift to durophagy due to biomechanical changes in its jaw cartilages. It remains to be seen if *H. francisci* undergoes a reduction in dietary diversity and increased niche specialization over ontogeny, with associated changes in feeding behavior and performance. A more detailed dietary analysis of neonate and juvenile *H. francisci* would be needed to determine whether these changes occur.

Biomechanical modeling and performance testing provide a morphological and behavioral basis from which to interpret differences in organismal ecology. These analyses determined that *H. francisci* is capable of generating bite forces an order of magnitude higher than comparably sized *S. acanthias* (Huber and Motta, 2004) and that *H. francisci* applies bite force in a way suited for processing hard prey. Differences in the feeding performance of *H. francisci* and *S. acanthias* directly coincide with the different feeding niches they occupy (durophagy and piscivory, respectively; Alonso et al., 2002; Segura-Zarzosa et al., 1997). Therefore, these analyses are of utility for understanding the diversity of elasmobranch feeding mechanisms at numerous organismal levels (morphology, behavior, ecology), as well as the selective pressures involved in the evolution of these mechanisms.

Heterodontus francisci has the second highest mass-specific bite force of the cartilaginous fishes in which bite force has been measured or estimated (Huber et al., 2004; Huber and Motta, 2004; Weggelaar et al., 2004; D. R. Huber, M. N. Dean and A. P. Summers, unpublished). Relative to body mass, the hardest biting cartilaginous fish studied thus far is *H. colliei*, which is also durophagous (Ebert, 2003; Johnson, 1967). Neither *H. francisci* nor *H. colliei* were comparable in biting ability to the durophagous teleost fishes *C. schoepfi*, *L. maximus* and the sheepshead, *Archosargus probatocephalus*. The mass-specific bite forces of these teleost fishes, which possess a battery of anatomical specializations associated with durophagy (Clifton and Motta, 1998; Hernandez and Motta, 1997; Korff and Wainwright, 2004), were considerably higher than those of the durophagous cartilaginous fishes (Appendix I). Comparative materials testing of the hard prey items in the diets of these cartilaginous and teleost fishes would be required to determine the ecological relevance of these differences in bite force. Nonetheless, the bite forces of these fishes collectively indicate that high biting performance, in addition to anatomical specialization, are associated with the consumption of hard prey.

Conclusions

The heterodontiform sharks, as represented by the horn shark *H. francisci*, possess a unique combination of morphological and behavioral characteristics that enable them to consume hard prey. Although *H. francisci* bites harder than the average vertebrate of comparable size, on a mass-specific basis it is not the most powerful biter in the animal kingdom (Fig. 8). Reptiles, mammals, other fishes and even some birds are capable of performing as well as or better than *H. francisci* when body mass is accounted for. These data suggest that factors other than bite force magnitude play a significant role in prey capture and processing ability. For *H. francisci*, these factors are molariform teeth, robust jaws, a high leverage jaw-adducting mechanism, and long duration, cyclically applied bite forces. The durophagous feeding behavior of *H. francisci* is reflected in its extensive ethmoidal articulation bracing the anterior portion of the upper jaw against the chondrocranium during prey capture and processing. Although *in situ* bite force measurements provided valuable information regarding its feeding behavior and ecology, theoretical estimates and restrained bite force measurements were the most effective means of estimating maximum bite force, depending on the availability of deceased specimens and live individuals. Because only a few investigations of biting performance in cartilaginous fishes have been made (Evans and Gilbert, 1971; Huber et al., 2004; Huber and Motta, 2004; Snodgrass and Gilbert, 1967; Weggelaar et al., 2004), little is known about the role that bite force plays in the ecological and evolutionary success of sharks. Combining theoretical and performance analyses provides the basis for an in-depth understanding of the link between morphology, behavior and ecology in sharks, and the role that biomechanics plays in the form and function of shark feeding mechanisms.

Appendix I

Vertebrate group	Source	Specific name	Common name	Anterior bite force (N)	Mass (g)	Residual bite force
Mammals	Ringqvist (1972)	*Homo sapiens*	Human	294	55 000	−1.21
	Robins (1977)	*Rattus norvegicus*	Norway rat	47	555	0.06
	Thomason et al. (1990)	*Didelphis virginiana*	North American opposum	442	5000	1.13
	Binder and Van Valkenburgh (2000)*	*Crocuta crocuta*	Spotted hyena	242	20 700	−0.74
		Crocuta crocuta	Spotted hyena	2195	292 000	0.05
	Thompson et al. (2003)	*Monodelphis domestica*	Short-tailed opposum	21	90	0.32
	Wroe et al. (2005)	*Acinonyx jubatus*	Cheetah	472	29 500	−0.15
		Alopex lagopus	Arctic fox	178	8200	−0.40
		Canis alpinus	Dhole	314	16 500	−0.21
		Canis aureus	Golden jackal	165	7700	−0.45
		Canis latrans	Coyote	275	19 800	−0.53
		Canis lupus dingo	Dingo	313	17 500	−0.25
		Canis lupus hallstromi	Singing dog	235	12 300	−0.36
		Canis lupus lupus	Grey wolf	593	34 700	0.01
		Dasyurus maculatus	Spotted-tailed quoll	153	3000	0.15
		Dasyurus viverrinus	Eastern quoll	65	870	0.02
		Felis concolor	Cougar	472	34 500	−0.28
		Felis sylvestris	Wild cat	56	2800	−1.04
		Felis yagouaroundi	Jaguarundi	127	7100	−0.73
		Gennetta tigrinum	Striped genet	73	6200	−1.32
		Hyaena hyaena	Brown hyena	545	40 800	−0.20
		Lycaon pictus	African hunting dog	428	18 900	0.06
		Lynx rufus	Bobcat	98	2900	−0.37
		Meles meles	European badger	244	11 400	−0.25
		Neofelis nebulosa	Clouded leopard	595	34 400	0.01
		Panthera leo	Lion	1768	294 600	−0.22
		Panthera onca	Jaguar	1014	83 200	0.05
		Panthera pardus	Leopard	467	43 100	−0.43
		Panthera tigris	Tiger	1525	186 900	−0.07
		Proteles cristatus	Aardwolf	151	9300	−0.70
		Sarcophilus harrisii	Tasmanian devil	418	12 000	0.38
		Thylacinus cynocephalus	Tasmanian wolf	808	41 700	0.28
		Urocyon cineroargentus	American grey fox	114	5300	−0.62
		Ursus americanus	Black bear	751	128 800	−0.67
		Ursus arctos	Brown bear	312	77 200	−1.42
		Ursus thibetanus	Asiatic bear	244	11 400	−0.25
		Vulpes vulpes	Red fox	164	8100	−0.51
Reptiles	Cleuren et al. (1995)	*Caiman crocodilus*	Spectacled caiman	70	1500	−0.28
	Herrel et al. (1999)	*Gallotia galloti*	Canary Island lizard	109	58	2.73
	Herrel et al. (2001)	*Xenosaurus grandis*	Knob-scaled lizard	12	17	1.09
		Xenosaurus newmanorum	Crevice-dwelling lizard	19	27	1.27
		Xenosaurus platyceps	Crocodile lizard	20	25	0.91
	Herrel et al. (2002)	*Amyda cartilaginea*	Asian softshell turtle	210	937	1.44
		Apalone ferox	Florida softshell turtle	42	114	0.99
		Apalone spinifera	Spiny softshell turtle	12	260	−1.17
		Callagur borneoensis	Painted terrapin	147	10 065	−0.79
		Chelus fimbriatus	Mata mata	5	405	−2.62
		Chelydra serpentina	Snapping turtle	209	3940	0.35
		Chinemys reevesii	Reeve's turtle	20	137	−0.07
		Dogania subplana	Malayan softshell turtle	37	328	0.05
		Elseya novaeguineae	New Guinea snapping turtle	35	743	−0.64
		Emydura subglobosa	Red-bellied short-necked turtle	2	119	−2.86
		Geoemyda spengleri	Black breasted leaf turtle	12	126	−0.64
		Heosemys grandis	Giant Asian pond turtle	102	2866	−0.31
		Kinosternon scorpioides	Scorpion mud turtle	38	214	0.41
		Kinosternon subrubrum	Mississippi mud turtle	35	133	0.66
		Macrochelys temminckii	Alligator snapping turtle	158	388	1.75
		Orlitia borneensis	Malaysian giant turtle	117	3818	−0.34

Table continued on next page.

Appendix I. *Continued*

Vertebrate group	Source	Specific name	Common name	Anterior bite force (N)	Mass (g)	Residual bite force
Reptiles	Herrel et al. (2002) *continued*	*Pelodiscus sinensis*	Chinese softshell turtle	59	305	0.70
		Pelomedusa subrufa	African helmeted turtle	8	224	−1.59
		Phrynops nasutus	Common toad-headed turtle	432	1752	1.89
		Platemys platycephala	Twist-necked turtle	7	245	−1.80
		Platysternon megacephalum	Big-headed turtle	42	137	0.86
		Staurotypus salvinii	Pacific coast giant musk turtle	252	743	1.84
		Staurotypus triporcatus	Mexican giant musk turtle	139	600	1.25
		Sternotherus carinatus	Razorback musk turtle	109	276	1.55
		Sternotherus odoratus	Common musk turtle	31	321	−0.16
		Terrapene carolina	Box turtle	25	361	−0.51
		Testudo horsfieldii	Russian tortoise	18	373	−0.93
		Trachemys scripta	Common slider turtle	15	235	−0.82
	Erickson et al. (2004)*	*Alligator mississippiensis*	American alligator	217	1650	1.06
		Alligator mississippiensis	American alligator	13 172	242 700	2.48
Birds	van der Meijj and Bout (2004)	*Amadina erythrocephala*	Red-headed finch	4	23	−0.74
		Amadina fasciata	Cut-throat finch	5	19	−0.24
		Carduelis chloris	European greenfinch	14	28	0.64
		Carduelis flammea	Common redpoll	3	13	−0.70
		Carduelis sinica	Grey-capped greenfinch	8	20	0.26
		Carduelis spinus	Eurasian siskin	3	13	−0.63
		Carpodacus erythrinus	Common rosefinch	6	22	−0.11
		Chloebia gouldia	Gouldian finch	4	15	−0.40
		Eophona migratoria	Yellow-billed grosbeak	36	52	1.41
		Erythrura trichroa	Blue-faced parrotfinch	5	13	0.02
		Estrilda troglodytes	Black-rumped waxbill	1	7	−1.52
		Hypargos niveoguttatus	Peter's twinspot	3	16	−0.80
		Lagonosticta senegala	Red-billed firefinch	1	7	−1.35
		Lonchura fringilloides	Magpie munia	5	16	−0.19
		Lonchura pallida	Pale-headed munia	3	13	−0.56
		Lonchura punctulata	Scaly-breasted munia	4	12	−0.36
		Mycerobas affinis	Collared grosbeak	38	70	1.24
		Neochima modesta	Plum-headed finch	2	13	−1.20
		Neochima ruficauda	Star finch	2	12	−1.07
		Padda oryzivora	Java sparrow	10	30	0.15
		Phoephila acuticauda	Long-tailed finch	3	8	−0.53
		Poephila cincta	Black-throated finch	3	16	−1.04
		Pyrrhula pyrrhula	Eurasian bullfinch	5	21	−0.41
		Pytilia hypogrammica	Red-faced pytilia	3	15	−0.75
		Rhodopechys obsoleta	Desert finch	6	23	−0.12
		Serinus leucopygius	White-rumped seedeater	2	10	−0.89
		Serinus mozambicus	Yellow-fronted canary	3	12	−0.66
		Serinus sulphuratus	Brimstone canary	12	18	0.80
		Taeniopygia bichenovi	Double-barred finch	2	10	−1.03
		Taenopygia guttata	Zebra finch	4	23	−0.77
		Uraeginthus bengalus	Red-cheeked cordonblue	1	10	−1.54
Fish	Hernandez and Motta (1997)	*Archosargus probatocephalus*	Sheepshead	309	998	1.88
	Clifton and Motta (1998)	*Halichoeres bivittatus*	Slippery dick	5	19	−0.35
		Halichoeres garnoti	Yellowhead wrasse	10	21	0.49
		Halichoeres maculipinna	Clown wrasse	11	18	0.71
		Lachnolaimus maximus	Hogfish	290	209	2.97
		Thalassoma bifasciatum	Bluehead wrasse	5	7	0.47
	Huber and Motta (2004)	*Squalus acanthias*	Spiny dogfish	20	501	−1.09
	Huber et al. (2004); D. R. Huber, M. N. Dean and A. P. Summers (unpublished)	*Hydrolagus colliei*	White-spotted ratfish	87	870	0.96
	Present study	*Heterodontus francisci*	Horn shark	206	2948	0.54
	Korff and Wainwright (2004)	*Chilomycterus schoepfi*	Striped burrfish	380	180	3.42
	Weggelaar et al. (2004)*	*Carcharhinus limbatus*	Blacktip shark	32	1274	−0.04
		Carcharhinus limbatus	Blacktip shark	423	22 092	−1.15

*Two values are given for studies in which specimen body masses ranged over more than one order of magnitude

List of symbols and abbreviations

α, angle of incidence of the ethmoidal articulation force

A_{CS}, cross-sectional area

C, ceratohyal

CC, coracoarcualis

CH, coracohyoideus

CHD, dorsal hyoid constrictor

CHV, ventral hyoid constrictor

CM, coracomandibularis

CO, coracoid bar

E, ethmoidal articulation

F, force

F_B, bite reaction force

F_E, ethmoidal articulation force

F_H, hyomandibular articulation force

F_{JR}, jaw joint reaction force,

F_{LJ}, static equilibrium of forces acting on the lower jaw

$F_{PO-\alpha}$, preorbitalis-α force

F_{QM-PO}, quadratomandibularis–preorbitalis complex force

$F_{QM-\gamma}$, quadratomandibularis-γ force

F_R, resultant jaw adducting force

F_{UJ}, static equilibrium of forces acting on the lower jaw

H, hyomandibula

HM, hyomandibulo-mandibularis

I, impulse

IMD, intermandibularis

LH, levator hyomandibularis

LJ, lower jaw

LP, levator palatoquadrati

O, orbital ariculation

P, postorbital articulation

P_0, theoretical maximum tetanic tension

PO-α, preorbitalis-α

QM–PO complex, quadratomandibularis–preorbitalis complex

QM-γ, quadratomandibularis-γ

T_{sp}, specific tension

UJ, upper jaw

VSBC, ventral superficial branchial constrictor

References

Aguirre, L. F., Herrel, A., Van Damme, R. and Matthysen, E. (2003). The implications of food hardness for diet in bats. *Funct. Ecol.* **17**, 201-212.

Aidley, D. J. (1998). *Physiology of Excitable Cells*. Cambridge: Cambridge University Press.

Alonso, M. K., Crespo, E. A., Garcia, N. A., Pedraza, S. N., Mariotti, P. A. and Mora, N. J. (2002). Fishery and ontogenetic driven changes in the diet of the spiny dogfish, *Squalus acanthias*, in Patagonian waters, Argentina. *Environ. Biol. Fish.* **63**, 193-202.

Askew, G. N. and Marsh, R. L. (1997). The effects of length trajectory on the mechanical power output of mouse skeletal muscles. *J. Exp. Biol.* **200**, 3119-3131.

Bemis, W. E. and Lauder, G. V. (1986). Morphology and function of the feeding apparatus of the lungfish, *Lepidosiren paradoxa* (Dipnoi). *J. Morphol.* **187**, 81-108.

Berra, T. (2001). *Freshwater Fish Distribution*. San Diego, CA: Academic Press.

Binder, W. J. and Van Valkenburgh, B. V. (2000). Development of bite strength and feeding behavior in juvenile spotted hyenas (*Crocuta crocuta*). *J. Zool.* **252**, 273-283.

Cappetta, H. (1987). *Chondrichthyes II: Mesozoic and Cenozoic Elasmobranchii*. Stuttgart: Gustav Fischer Verlag.

Carroll, R. L. (1988). *Vertebrate Paleontology and Evolution*. New York: W. H. Freeman and Co.

Carter, D. R. and Wong, M. (2003). Modelling cartilage mechanobiology. *Philos. Trans. R. Soc. London Ser. B* **358**, 1461-1471.

Christoforou, A. P., Swanson, S. R. and Beckwith, S. W. (1989). Lateral impact of composite cylinders. In *Second Symposium on Composite Materials: Fatigue and Fracture*, vol. 2 (ed. P. A. Lagace), pp. 373-386. Cincinnati: American Society for Testing and Materials.

Cleuren, J., Aerts, P. and De Vree, F. (1995). Bite and joint force analysis in *Caiman crocodilus*. *Belg. J. Zool.* **125**, 79-94.

Clifton, K. B. and Motta, P. J. (1998). Feeding morphology, diet, and ecomorphological relationships among five Caribbean labrids (Teleostei, Labridae). *Copeia* **1998**, 953-966.

Compagno, L. J. V. (1984a). *Sharks of the World. An Annotated and Illustrated Catalogue of Shark Species Known to Date. Part 1, Hexanchiformes to Lamniformes*. Rome: Food and Agriculture Organization of the United Nations.

Compagno, L. J. V. (1984b). *Sharks of the World. An Annotated and Illustrated Catalogue of Shark Species Known to Date. Part 2, Carcharhiniformes*. Rome: Food and Agriculture Organization of the United Nations.

Compagno, L. J. V. (1999). Checklist of living elasmobranchs. In *Sharks, Skates, and Rays: The Biology of Elasmobranch Fishes* (ed. W. C. Hamlett), pp. 471-498. Baltimore, MD: Johns Hopkins University Press.

Compagno, L. J. V. (2001). S*harks of the World. An Annotated and Illustrated Catalogue of Shark Species Known to Date. Vol. 2. Bullhead, Mackerel, and Carpet Sharks (Heterodontiformes, Lamniformes, and Orectolobiformes)*. Rome: Food and Agriculture Organization of the United Nations.

Daniel, J. F. (1915). The anatomy of *Heterodontus francisci* II: the endoskeleton. *J. Morphol.* **26**, 447-493.

Durie, C. J. and Turingan, R. G. (2001). Relationship between durophagy and feeding biomechanics in gray triggerfish, *Balistes capriscus*: intraspecific variation in ecological morphology. *Fla. Sci.* **64**, 20-28.

Ebert, D. A. (2003). *Sharks, Rays, and Chimaeras of California*. Berkeley: University of California Press.

Edmonds, M. A., Motta, P. J. and Hueter, R. E. (2001). Food capture kinematics of the suction feeding horn shark *Heterodontus francisci*. *Environ. Biol. Fishes* **62**, 415-427.

Ellers, O., Johnson, A. S. and Moberg, P. E. (1998). Structural strengthening of urchin skeletons by collagenous sutural ligaments. *Biol. Bull.* **195**, 136-144.

Erickson, G. M., Lappin, A. K., Parker, T. and Vliet, K. A. (2004). Comparison of bite performance between long-term captive and wild American alligators *Alligator mississippiensis*. *J. Zool.* **262**, 21-28.

Evans, W. R. and Gilbert, P. W. (1971). The force of bites by the silky shark (*Carcharhinus falciformis*) measured under field conditions. San Diego: Naval Undersea Research and Development Center.

Frazzetta, T. H. (1994). Feeding mechanisms in sharks and other elasmobranchs. *Adv. Comp. Environ. Physiol.* **18**, 31-57.

Gadow, H. (1888). On the modifications of the first and second visceral arches, with special reference to the homologies of the auditory ossicles. *Philos. Trans. R. Soc. London Ser. B* **179**, 451-485.

Gregory, W. K. (1904). The relations of the anterior visceral arches to the chondrocranium. *Biol. Bull.* **7**, 55-69.

Hernandez, L. P. and Motta, P. J. (1997). Trophic consequences of differential performance: ontogeny of oral jaw-crushing performance in the sheepshead, *Archosargus probatocephalus* (Teleostei, Sparidae). *J. Zool.* **243**, 737-756.

Herrel, A., Aerts, P. and DeVree, F. (1998). Ecomorphology of the lizard feeding apparatus: a modeling approach. *Neth. J. Zool.* **48**, 1-25.

Herrel, A., Spithoven, L., Van Damme, R. and De Vree, F. (1999). Sexual dimorphism of head size in *Gallotia galloti*: Testing the niche divergence hypothesis by functional analyses. *Funct. Ecol.* **13**, 289-297.

Herrel, A., Grauw, E. and Lemos-Espinal, J. A. (2001). Head shape and bite performance in xenosaurid lizards. *J. Exp. Zool.* **290**, 101-107.

Herrel, A., O'Reilly, J. C. and Richmond, A. M. (2002). Evolution of bite performance in turtles. *J. Evol. Biol.* **15**, 1083-1094.

Hibbeler, R. C. (2004). *Engineering Mechanics: Statics.* 10th edition. Upper Saddle River, NJ: Prentice Hall.

Huber, D. R. and Motta, P. J. (2004). Comparative analysis of methods for determining bite force in the spiny dogfish *Squalus acanthias*. *J. Exp. Zool.* **301**, 26-37.

Huber, D. R., Dean, M. N. and Summers, A. P. (2004). The crushing bite of the water bunny *Hydrolagus colliei*. *Integr. Comp. Biol.* **44**, 573.

Hwang, W. and Han, K. S. (1989). Fatigue of composite materials: damage model and life prediction. In *Second Symposium on Composite Materials: Fatigue and Fracture*, vol. 2 (ed. P. A. Lagace), pp. 87-102. Cincinnati: American Society for Testing and Materials.

Johnson, A. G. (1967). Biology of the ratfish, *Hydrolagus colliei* (Lay and Bennett). *M.Sc. Thesis.* Oregon State University, Oregon, USA.

Johnston, I. A. (1980). Contractile properties of fish fast muscle fibers. *Mar. Biol. Lett.* **1**, 323-328.

Josephson, R. K. (1999). Dissecting muscle power output. *J. Exp. Biol.* **202**, 3369-3375.

Kiltie, R. A. (1982). Bite force as a basis for niche diversification between rain forest peccaries (*Tayassu tajacu* and *T. pecari*). *Biotropica* **14**, 188-195.

Koolstra, J. H., Van Eijden, T. M. G. J., Weijs, W. A. and Naeije, M. (1988). A three-dimensional mathematical model of the human masticatory system predicting maximum possible bite forces. *J. Biomech.* **21**, 563-576.

Korff, W. L. and Wainwright, P. C. (2004). Motor pattern control for increasing crushing force in the striped burrfish (*Chilomycterus schoepfi*). *Zoology* **107**, 335-346.

Lou, F., Curtin, N. A. and Woledge, R. C. (2002). Isometric and isovelocity contractile performance of red muscle fibers from the dogfish *Scyliorhinus canicula*. *J. Exp. Biol.* **205**, 1585-1595.

Maisey, J. G. (1980). An evaluation of jaw suspension in sharks. *Amer. Mus. Novit.* **2703**, 1-17.

Maisey, J. G. (1985). Cranial morphology of the fossil elasmobranch *Synechodus dubrisiensis*. *Amer. Mus. Novit.* **2804**, 1-28.

Moss, S. A. (1972). The feeding mechanism of sharks of the family Carcharhinidae. *J. Zool. Lond.* **167**, 423-436.

Moss, S. A. (1977). Feeding mechanisms in sharks. *Am. Zool.* **17**, 355-364.

Motta, P. J. (2004). Prey capture behavior and feeding mechanics of elasmobranchs. In *Biology of Sharks and Their Relatives* (ed. J. Carrier, J. Musick and M. Heithaus), pp. 165-202. Boca Raton: CRC Press.

Motta, P. J. and Wilga, C. A. D. (1995). Anatomy of the feeding apparatus of the lemon shark, *Negaprion brevirostris*. *J. Morphol.* **226**, 309-329.

Motta, P. J. and Wilga, C. D. (1999). Anatomy of the feeding apparatus of the nurse shark, *Ginglymostoma cirratum*. *J. Morphol.* **241**, 33-60.

Motta, P. J., Tricas, T. C., Hueter, R. E. and Summers, A. P. (1997). Feeding mechanism and functional morphology of the jaws of the lemon shark *Negaprion brevirostris* (Chondrichthyes, Carcharhinidae). *J. Exp. Biol.* **2765**-2780.

Motta, P. J., Hueter, R. E., Tricas, T. C. and Summers, A. P. (2002). Kinematic analysis of suction feeding in the nurse shark, *Ginglymostoma cirratum* (Orectolobiformes, Ginglymostomatidae). *Copeia* **1**, 24-38.

Moy-Thomas, J. A. and Miles, R. S. (1971). *Paleozoic Fishes*. London: Chapman and Hall.

Muller, M. and Osse, J. W. M. (1984). Hydrodynamics of suction feeding in fish. *Trans. Zool. Soc. Lond.* **37**, 51-135.

Nauwelaerts, S. and Aerts, P. (2003). Propulsive impulse as a covarying performance measure in the comparison of the kinematics of swimming and jumping in frogs. *J. Exp. Biol.* **206**, 4341-4351.

Nobiling, G. (1977). Die Biomechanik des Kiefferapparates beim Stierkpfhai (*Heterodontus portusjacksoni* = *Heterodontus philippi*). *Adv. Anat. Embryol. Cell Biol.* **52**, 1-52.

Provan, J. W. and Zhai, Z. H. (1985). A review of fatigue crack initiation. In *Time-Dependent Fracture* (ed. A. S. Krausz), pp. 201-212. Dordrecht, The Netherlands: Martinus Nijhoff Publishers.

Quinn, G. P. and Keough, M. J. (2002). *Experimental Design and Data Analysis for Biologists.* Cambridge: Cambridge University Press.

Reif, W. E. (1976). Morphogenesis, pattern formation, and function of the dentition of *Heterodontus* (Selachii). *Zoomorphologie* **83**, 1-47.

Ringqvist, M. (1972). Isometric bite force and its relation to dimensions of the facial skeleton. *Acta Odontol. Scand.* **31**, 35-42.

Robins, M. W. (1977). Biting loads generated by the laboratory rat. *Arch. Oral Biol.* **22**, 43-47.

Sanford, C. P. and Wainwright, P. C. (2002). Use of sonomicrometry demonstrates the link between prey capture kinematics and suction pressure in largemouth bass. *J. Exp. Biol.* **205**, 3445-3457.

Schaeffer, B. (1967). Comments on elasmobranch evolution. In *Sharks, Skates, and Rays* (ed. P. W. Gilbert, R. F. Mathewson and D. P. Rall), pp. 3-35. Baltimore: Johns Hopkins Press.

Segura-Zarzosa, J. C., Abitia-Cardenas, L. A. and Galvan-Magana, F. (1997). Observations on the feeding habits of the shark *Heterodontus francisci* Girard 1854 (Chondrichthyes: Heterodontidae), in San Ignacio Lagoon, Baja California Sur, Mexico. *Ciencias Marinas* **23**, 111-128.

Shirai, S. (1996). Phylogenetic interrelationships of neoselachians (Chondrichthyes: Euselachii). In *Interrelationships of Fishes* (ed. M. L. J. Stiassny, L. R. Parenti, G. D. Johnson), pp. 9-34. San Diego: Academic Press.

Snodgrass, J. M. and Gilbert, P. W. (1967). A shark-bite meter. In *Sharks, Skates, and Rays* (ed. P. W. Gilbert, R. F. Mathewson and D. P. Rall), pp. 331-337. Baltimore: Johns Hopkins Press.

Stahl, B. J. (1988). Reconstruction of the head skeleton of the fossil elasmobranch, *Phoebodus heslerorum* (Pisces: Chondrichthyes). *Copeia* **4**, 827-1183.

Strong, W. R., Jr (1989). Behavioral ecology of horn sharks, *Heterodontus francisci*, at Santa Catalina Island, California, with emphasis on patterns of space utilization. *M.Sc. Thesis.* California State University at Long Beach, California, USA.

Summers, A. P., Ketcham, R. and Rowe, T. (2004). Structure and function of the horn shark (*Heterodontus francisci*) cranium through ontogeny: the development of a hard prey crusher. *J. Morphol.* **260**, 1-12.

Svanback, R., Wainwright, P. C. and Ferry-Graham, L. A. (2002). Linking cranial kinematics, buccal pressure, and suction feeding performance in largemouth bass. *Physiol. Biochem. Zool.* **75**, 532-543.

Taylor, L. R. (1972). A revision of the sharks of the family Heterodontidae. *Ph.D. Thesis.* University of California at San Diego, San Diego, USA.

Thomason, J. J., Russell, A. P. and Morgeli, M. (1990). Forces of biting, body size, and masticatory muscle tension in the opossum *Dedelphis virginiana*. *Can. J. Zool.* **68**, 318-324.

Thomason, J. J., Russell, A. P. and Morgeli, M. (1991). Cranial strength in relation to estimated biting forces in some mammals. *Can. J. Zool.* **69**, 2326-2333.

Thompson, E. N., Biknevicus, A. R. and German, R. Z. (2003). Ontogeny of feeding function in the gray short-tailed opossum *Monodelphis domestica*: empirical support for the constrained model of jaw biomechanics. *J. Exp. Biol.* **206**, 923-932.

Turingan, R. G. and Wainwright, P. C. (1993). Morphological and functional bases of durophagy in the queen triggerfish, *Balistes vetula* (Pisces, Tetradontiformes). *J. Morphol.* **215**, 101-118.

Turingan, R. G., Wainwright, P. C. and Hensley, D. A. (1995). Interpopulation variation in prey use and feeding biomechanics in Caribbean triggerfishes. *Oecologia* **102**, 296-304.

van der Meij, M. A. A. and Bout, R. G. (2004). Scaling of jaw muscle size and maximal bite force in finches. *J. Exp. Biol.* **207**, 2745-2753.

Van Leeuwen, J. L. and Muller, M. (1984). Optimum sucking techniques for predatory fish. *Trans. Zool. Soc. London* **37**, 137-169.

Verwaijen, D., Van Damme, R. and Herrel, A. (2002). Relationships between head size, bite force, prey handling efficiency and diet in two sympatric lacertid lizards. *Funct. Ecol.* **16**, 842-850.

Wainwright, P. C. (1988). Morphology and ecology: Functional basis of feeding constraints in Caribbean labrid fishes. *Ecology* **69**, 635-645.

Wainwright, P. C., Bellwood, D. R., Westneat, M. W., Grubich, J. R. and Hoey, A. S. (2004). A functional morphospace for the skull of labrid fishes: patterns of diversity in a complex biomechanical system. *Biol. J. Linn. Soc.* **82**, 1-25.

Weggelaar, C. W., Huber, D. R. and Motta, P. J. (2004). Scaling of bite

force in the blacktip shark *Carcharhinus limbatus*. *Integr. Comp. Biol.* **44**, 662.

Westneat, M. W. (2004). Evolution of levers and linkages in the feeding mechanisms of fishes. *Integr. Comp. Biol.* **44**, 278-289.

Wiersma, J. H. (2001). Maximum estimated bite force, skull morphology, and primary prey size in North American carnivores. MSc thesis, Laurentian University, Ontario, Canada.

Wilga, C. D. (2002). A functional analysis of jaw suspension in elasmobranchs. *Biol. J. Linn. Soc.* **75**, 483-502.

Wilga, C. D. and Motta, P. J. (1998). Conservation and variation in the feeding mechanism of the spiny dogfish *Squalus acanthias*. *J. Exp. Biol.* **201**, 1345-1358.

Wilga, C. A. D. and Motta, P. J. (2000). Durophagy in sharks: feeding mechanics of the hammerhead *Sphyrna tiburo*. *J. Exp. Biol.* **203**, 2781-2796.

Wilga, C. D., Wainwright, P. C. and Motta, P. J. (2000). Evolution of jaw depression mechanics in aquatic vertebrates: insights from Chondrichthyes. *Biol. J. Linn. Soc.* **71**, 165-185.

Wilga, C. D., Hueter, R. E., Waiwright, P. C. and Motta, P. J. (2001). Evolution of upper jaw protrusion mechanisms in elasmobranchs. *Am. Zool.* **41**, 1248-1257.

Wroe, S., McHenry, C. and Thomason, J. (2005). Bite club: comparative bite force in big biting mammals and the prediction of predatory behavior in fossil taxa. *Proc. R. Soc. London Ser. B* **272**, 619-625.